Lawrence Berkeley Laboratory
UNIVERSITY OF CALIFORNIA

ENERGY & ENVIRONMENT DIVISION

Submitted for publication

FLAT FLAME BURNER ANALYSES

P. J. Pagni, A. Ortega and R. Toossi

October 1979

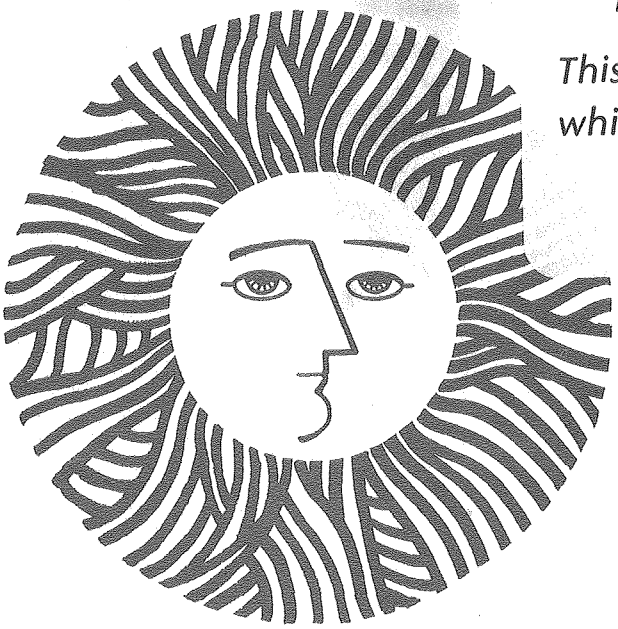

Prepared for the U.S. Department of Energy under Contract W-7405-ENG-48

DISCLAIMER

Flat Flame Burner Analyses

by

P. J. Pagni, A. Ortega and R. Toossi
Department of Mechanical Engineering
and
Lawrence Berkeley Laboratory
University of California
Berkeley, CA 94720

UCB-FRG-79-3/WSS-CI-79-47

October 1979

This work was supported by the U. S. Department of Energy
under Contract W-7405-ENG-48

The authors are grateful for support from the National Bureau of Standards - Fire Research Center and from the Products Research Committee. The conclusions drawn herein are those of the authors and not of the Products Research Committee nor the National Bureau of Standards.

Flat Flame Burner Analyses

by

P. J. Pagni, A. Ortega and R. Toossi
Department of Mechanical Engineering
and
Lawrence Berkeley Laboratory
University of California
Berkeley, CA 94720

Abstract

Velocity and temperature fields in the sintered material surrounding an embedded cooling coil in a Kaskan type flat flame burner are predicted. An approximate two-dimensional velocity field is obtained in closed form using a potential flow analogy. The velocity profile above the burner surface will be flat if the distance from the burner surface to the plane of the coil is sufficiently large that the coil wake is ameliorated. Quantitative results for this minimum distance are presented. Several approximations to the temperature field are discussed. Detailed temperature profiles are given for the simplest - one-dimensional with uniform velcotiy - and the most complex - two-dimensional with potential flow velocity field. The influence of the burner and cooling geometries, fuel type and stoichiometry, flow rate, ambient and cooling water temperatures and sintered material properties, are all described by a small set of dimensionless parameters. Optimization of burner performance in terms of these parameters is discussed. It is hoped that the results will be useful in the design of burners for flame structure studies.

Introduction

A Kaskan type flat flame burner [1] consists of a porous metal disk through which a premixed combustible mixture flows at a controlled rate. A flame is stabilized downstream of (above) the burner by heat transfer to the disk. Steady state can be established over a fairly wide range of flow rates and equivalence ratios by embedding a copper, water cooled, spiral coil within the sintered bronze disk. The purpose of this device is to create an approximately one-dimensional reaction zone for well-controlled experimental studies of chemical kinetics.

During the operation of one such burner [2], the pattern of the cooling coil appeared in the flame as concentric bright and dark regions. This strange behavior was observed for propane-air and acetylene-air flames over a wide range of flow rates and equivalence ratios. Such a rippled flame was clearly not the desired "flat" flame. In order to understand this phenomenon and to define design criteria for burners which would produce, as nearly as possible, flat flames, a detailed theoretical study of the velocity and temperature profiles at the exit plane of the porous disk is described here.

Velocity and temperature fields for steady laminar flow of a premixed gas within the porous disk are developed. The appropriate momentum equation is Darcy's law. Natural convection is neglected due to small Rayleigh numbers [3]. The following additional assumptions are made: fluid properties are constant as well as the permeability and thermal conductivity of the disk; the cooling water maintains the entire coil at a constant temperature, T_w, equal to the average of the inlet and outlet water temperatures; the radius of curvature of the coil (or the burner radius) is large compared to the radius of the copper tubing from which the coil is constructed so that a two-dimensional Cartesian field exists around each element of the coil; the

temperature of the gas is the same as the temperature of the disk at each point within the disk [4].

Due to the neglect of buoyancy and the assumption of constant viscosity and permeability, the momentum and energy equations are uncoupled and treated separately. After some manipulation, Darcy's law results in Laplace's equation for the stream function. The two-dimensional elliptic energy equation and boundary conditions are discretized using finite-difference techniques and the resulting system of linear equations is solved using Gauss-Seidel iteration. For comparison, the limit of one-dimensional fluid flow with an upstream boundary condition of $T = T_w$ at the center plane of the cooling coil gives an analytic expression for the temperature distribution. In the numerical solution the velocity was not assumed constant and the boundary condition was $T = T_w$ on the cooling coil contour.

Velocity Distribution

Consider the two-dimensional schematic shown in Fig. 1. Assuming equal spacing, there exists a line of symmetry between successive cylinders of the cooling coil. At this line of symmetry and on the x-axis, the y-component of the velocity, V, equals zero. The upstream and downstream boundary conditions are allowed to go to infinity. To resolve the velocity distribution the problem can be considered as two-dimensional potential flow of a uniform stream over a circular cylinder with the flow constrained by parallel impermeable walls. Darcy's law can be written in the following form [5],

$$U = \frac{-\varepsilon}{\mu} \frac{\partial P}{\partial x} \quad , \quad V = \frac{-\varepsilon}{\mu} \frac{\partial P}{\partial y} \tag{1}$$

Introducing the stream function, i.e., $U = \frac{\partial \psi}{\partial y}$, $V = \frac{\partial \psi}{\partial x}$, and cross-differentiating the momentum equations to eliminate the pressure, the result is Laplace's equation,

$$\frac{\partial^2 \psi}{\partial x^2} + \frac{\partial^2 \psi}{\partial y^2} = 0 \quad .$$

As a first approximation, solve the velocity field for the limiting case $H/D = \infty$. Now the problem is simply two-dimensional potential flow of a uniform stream over a circular cylinder whose solution is well-known [6]. The complex potential of a circular cylinder placed in a uniform stream at U_∞ is

$$w = U_\infty (z + D^2/4z) \tag{2}$$

where w is the complex potential and $z = x + iy$. The velocity components can be found from,

$$\frac{dw}{dz} = U - iV = U_\infty \left(1 - \frac{D^2}{4z^2}\right) \quad .$$

In dimensionless form, the velocity components are

$$\bar{U} = \frac{U}{U_\infty} = 1 - \frac{\bar{x}^2 - \bar{y}^2}{4(\bar{x}^2 + \bar{y}^2)^2} \quad , \quad \bar{V} = \frac{V}{U_\infty} = \frac{-\bar{x}\bar{y}}{2(\bar{x}^2 + \bar{y}^2)^2}$$

where $\bar{x} = x/D$ and $\bar{y} = y/D$.

The dimensionless speed is

$$\frac{S}{U_\infty} = (\bar{U}^2 + \bar{V}^2)^{1/2} = \left[\left(1 - \frac{\bar{x}^2 - \bar{y}^2}{4(\bar{x}^2 + \bar{y}^2)^2}\right)^2 + \left(\frac{-\bar{x}\bar{y}}{2(\bar{x}^2 + \bar{y}^2)^2}\right)^2\right]^{1/2}$$

The result in this limiting case is that the velocity profile at the disk exit plane will be flat to within 1% provided the exit plane is five coil diameters downstream of the plane of the cooling coil.

Now consider the more general case of an arbitrary separation between successive tubes within the spiral coil. The constraints due to the walls at $\bar{y} = \pm H/2D$ (lines of symmetry) may be replaced [7] by an infinite series of images situated at the distances $\pm$ in H where $n = 0, \pm 1, \pm 2, \ldots$ The cylinder and its boundary walls are represented by the superposition of flow due to a uniform stream and flows due to a doublet located at the center

of each of the coils. The complex potential for an image of order n is

$$w_n = M \frac{1}{z \pm inH} + U_\infty z$$

where M is the as yet undefined strength of the doublet. The total complex potential for the images and the real cylinder is

$$w = U_\infty z + M[\frac{1}{z} + \sum_{n=1}^{\infty} (\frac{1}{z - inH} + \frac{1}{z + inH})]$$

Now use the identity,

$$\coth (\frac{\pi z}{H}) = \frac{1}{\pi z/H} + \frac{2\pi z}{H} \sum_{n=1}^{\infty} \frac{1}{(n\pi)^2 + (\pi z/H)^2} \tag{3}$$

to eliminate the series.

$$\frac{1}{z - inH} + \frac{1}{z + inH} = \frac{2z}{z^2 + n^2H^2} = \frac{2z\pi^2}{H^2} (\frac{1}{(n\pi)^2 + (\pi z/H)^2}) \quad .$$

Thus,

$$w = U_\infty z + (M\pi/H) \coth (\pi z/H) \quad . \tag{4}$$

The unknown constant M is obtained from the boundary condition at the rear stagnation point, $\bar{x} = \frac{1}{2}$ and $\bar{y} = 0$,

$$\frac{d\bar{w}}{d\bar{z}} (\tfrac{1}{2},0) = \bar{U}(\tfrac{1}{2},0) - i\bar{V}(\tfrac{1}{2},0) = 0 \quad ,$$

where $\bar{w} = w/U_\infty D$ and $\bar{z} = z/D$. From Eq. (4)

$$\bar{w} = \bar{z} + \frac{M\pi}{U_\infty DH} \coth (\pi \bar{z}\, D/H).$$

Applying the condition gives

$$M = \frac{U_\infty H^2}{\pi^2} \sinh^2 (\pi D/2H) \quad .$$

The nondimensional complex potential is then

$$\bar{w} = \bar{z} + (H/\pi D)\ \sinh^2(\pi D/2H)\ \coth(\pi D\bar{z}/H) \quad . \tag{5}$$

In the limit $H/D \to \infty$

$$\sinh\left(\frac{\pi D}{2H}\right) \to \frac{\pi D}{2H} \quad \text{and} \quad \coth\left(\frac{\pi \bar{z} D}{H}\right) \to \frac{H}{\pi \bar{z} D}$$

so that the general solution, Eq. (5), approaches the previously obtained limiting case for very large H/D, Eq. (2)

$$\bar{w} = \bar{z} + (4\bar{z})^{-1} \quad .$$

The dimensionless velocity components and dimensionless speed can now be determined from Eq. (5) as functions of $\bar{z}$ and H/D,

$$\frac{d\bar{w}}{d\bar{z}} = \bar{U} - i\bar{V} = \left[1 - \frac{\sinh^2(\pi D/2H)}{\sinh^2(\pi z D/H)}\right]$$

$$\frac{S}{U_\infty} = (\bar{U}^2 + \bar{V}^2)^{\frac{1}{2}} = \left\{\left(\mathrm{Re}\left[1 - \frac{\sinh^2(\pi D/2H)}{\sinh^2(\pi \bar{z} D/H)}\right]\right)^2 + \left(-\mathrm{Im}\left[1 - \frac{\sinh^2(\pi D/2H)}{\sinh^2(\pi \bar{z} D/H)}\right]\right)^2\right\}^{\frac{1}{2}} \tag{6}$$

Figure 2 shows the streamlines of Eq. (5) and Fig. 3 the constant speed contours for H/D = 2, i.e., the free space separating tubes in the spiral equals the tube diameter.

The streamlines shown in Fig. 2 indicate how quickly uniformity is achieved downstream of the cylinder. Comparison with a similar plot for $H/D \to \infty$ indicates that the closer the tubes in the coil (H/D smaller) the shorter is the coil wake. The optimum coil would be a tightly wound spiral of small tube diameter (since all distances scale with tube diameters). To quantify this effect consider the constant speed contours shown in Fig. 3. The maximum velocities occur in the plane of the coil, $\bar{x} = 0$, where some inaccuracies are introduced by the method of images.

The $\psi = 0$ streamline defines the contour of the cylindrical coil tube. Since this method is not exact, the contour is elliptical rather than circular. However, for physically interesting H/D's this deformation is quite small. Only the portion of the flow field directly adjacent to the tube contour is affected. Since it is of interest to determine velocity nonuniformity far downstream, this distortion effect is negligible.

For the H/D = 2 of Fig. 3, $S = U_\infty$ to within $\pm$ 1% throughout the flow field for $\bar{x} > 1.82$. The location of the maximum deviation is on the $\bar{y}$ axis. Based on this criterion, the velocity on the $\bar{y}$ axis within 1% of U_∞, Fig. 4 gives the distance the exit plane must be placed downstream of the central plane of the coil to achieve a flat profile as a function of H/D. Unrealistically large H/D are required before the asymptote, $\bar{x} = 5$, is reached. The practical range of $1.5 > H/D > 4.5$, shown in the insert, is well fit by

$$\bar{x}_{min} = L/D = 0.9 + 0.45\ H/D \tag{7}$$

where L is the minimum permissible distance between the exit plane and the coil plane.

In the rippled flame case discussed in the introduction, a 1/4" tube was embedded at the center of a 3/4" disk; approximately 3/4" separated successive coil centers. Thus, $H/D \approx 3$ with $L/D \approx 1.5$ which is considerably less than the required $L/D \approx 2.3$ from Fig. 4. Approximately a 20% change in velocity would have existed from $\bar{y} = 0$ to $\bar{y} = 1.5$ with repetitions across the burner possibly creating the pattern observed. Subsequent burners were designed with 1/2" tubes, centered 7/16" below the surface of a 5/8" thick disk; approximately 5/16" separated coil centers. Here H/D = 2.5 with L/D = 3.5, considerably more than the 2.1 required by Fig. 4. No pattern was observed in the flames on this burner. Cold flow velocity measurements also indicated a flat velocity profile at the disk exit plane.

In addition, an analog electric field device using conducting paper was employed to investigate the approximation of placing the upstream boundary at infinity. Variation of the upstream distance from the cooling coil was found to have no effect on the downstream flow field for $\bar{x} \geq 1$. The important practical consequence is that the sinter material upstream of the cooling coil has no significant influence on the fluid mechanics within the disk downstream of the coil. Perhaps the simpler technique of soldering the coil to the lower disk surface, rather than sintering it within the disk, would suffice.

Temperature Distribution

The problem of the temperature distribution within the porous disk is strongly coupled to the more complicated problem of the temperature, velocity and species fields in the reaction zone downstream of the disk exit [8,9]. As a first approximation, it is assumed here that the heat flux from the flame to the disk, $\dot{q}''_{f\ell}$, is known and uniform over the disk exit plane.

Consider first the simplest case of no y component of velocity and ρs uniform everywhere within the disk. The coil is shrunk to a cooling sheet at $x = 0$, assumed to be uniform at T_w. The periphery of the disk is perfectly insulated. The problem is steady one-dimensional conduction with flow subject to a Dirichlét condition at $x = 0$, the plane of the coil, and a Neumann condition at $x = L$, the disk exit plane beneath the flame. The nondimensional problem is

$$\frac{d^2\bar{T}}{d\bar{x}^2} - Pe\,\frac{d\bar{T}}{d\bar{x}} = 0,$$

$$\bar{T}(0) = 0 \quad \text{and} \quad \frac{d\bar{T}}{d\bar{x}}(1) = 1 \quad ,$$

where $\bar{T} = \lambda_s(T - T_w)/\dot{q}''_{f\ell}L$, $Pe = \rho_u S_u c_{pg} L/\lambda_s$ and here $\bar{x} = x/L$.

The solution is

$$\bar{T}(\bar{x}) = [\exp(\bar{x}Pe) - 1]/[Pe \exp(Pe)] \quad . \tag{8}$$

Figure 5 shows the temperature field in the disk as given by Eq. (8) vs. $\bar{x}$ parameterized in Pe. The profile is approximately linear for Pe < 0.5, which is an upper limit to practical cases, at least for sintered metal disks. Ceramic systems would have lower λ_s and possibly higher Pe. For Pe $\leq$ 0.1, the surface temperature is within 5% of the simple linear value

$$T_u = T_w + \dot{q}''_{f\ell} L/\lambda_s \quad .$$

Figure 6 shows the disk surface temperature beneath the flame from Eq. (8) for any Pe. These results may have utility for experimental determinations of $\dot{q}''_{f\ell}$ from measurements of Tu.

A much more detailed study [2] has been made of the two-dimensional temperature field in the disk for the same flow and x boundary conditions, but with an unisolated disk periphery. The additional dimension ranges from 0 on the axis of the burner to r_b at the rim of the disk. The problem is steady, two-dimensional conduction with flow subject to the x boundary conditions listed above, with T finite at the origin and $\partial T'(1)/\partial T + Bi\,T'(1) = 0$. Here $T' = \lambda_s(T - T_\infty)/\dot{q}''_{f\ell}L$, $\bar{r} = r/r_b$ and $Bi = hr_b/\lambda_s$ where T_∞ is the average ambient gas temperature. The aspect ratio $a = L/r_b$ appears in the governing equation and the nondimensional water temperature enters at the upstream boundary condition. Only the results for the surface temperature as shown in Fig. 7 will be discussed here. The influence of Pe is essentially given by Fig. 6 and T'_w does not vary significantly from zero. However, these parameters are responsible for the nonunity centerline temperature for a = 0.3 or less where, indeed, Fig. 6 gives the centerline temperature for all rim conditions, i.e., all Bi. When a > 0.3 rim losses also drop the centerline temperature, but a much

larger than 0.3 is rare. Burners constructed here typically had $L \approx 1.1$ cm and $r_b \approx 3.5$ cm so that $a \approx 0.3$. The value of Bi in practical cases is more difficult to quantify. The most serious rim heat leak probably occurs when the conductivity of the solid material surrounding the disk is much greater than that of the sintered material, thus providing a short circuit from the surface beneath the flame to the cooling coil. The measured conductivity of the sintered material used here (95% Cu - 5% Sn with particle radii from 0.07 mm to 0.09 mm) was 7 Btu/hrft°F. When the disk was mounted in cast iron, $\lambda \approx 30$ Btu/hrft°F, significant rim loss was observed, while with various stainless steels, $\lambda \lesssim 9$ Btu/hrft°F, such losses were not apparent. If this short circuit effect is avoided, Bi < 1 can be expected and $[T'_u(0) - T'_u(1)]/T'_u(0) \leq 0.1$ as shown in Fig. 7.

Now consider the temperature field for the more realistic coil geometry described in the velocity distribution section. One can control the rim loss by insulation, so setting Bi = 0 then is reasonable. This has the advantage of returning considerations to the small Cartesian symmetry cell about a coil tube as shown in Fig. 1. The temperature field within the entire burner is then reconstructed with the assumption that the calculated pattern exists over every element of the spiraled coil. There is no strong radial variation in the Kaskan type burner as observed [10] in the older style rim cooled burners [11].

The velocity field given by Eq. (6) is assumed. The problem is steady, two-dimensional conduction with flow subject to the following conditions: insulated walls at $\bar{y} = 0$ and H/2D; constant flux, $\dot{q}''_{f\ell}$, at the downstream boundary, $\bar{x} = L/D$; constant temperature, T_∞, at the upstream boundary, $\bar{x} = -N/D$ and constant temperature, T_w, along the coil contour, $\bar{x}^2 + \bar{y}^2 = 1/4$. Thus, the nondimensional problem is:

$$\frac{L}{D}\left(\frac{\partial^2\bar{T}}{\partial\bar{x}^2}+\frac{\partial^2\bar{T}}{\partial\bar{y}^2}\right)-\mathrm{Pe}\left(\bar{U}\frac{\partial\bar{T}}{\partial\bar{x}}+\bar{V}\frac{\partial\bar{T}}{\partial\bar{y}}\right)=0 \qquad (9)$$

with

$$\bar{T}\,(-N/D,\bar{y})=\bar{T}_\infty\ , \qquad \frac{1}{2}<\bar{y}\le H/2D\ ,$$

$$\bar{T}\,(\bar{x}^2+\bar{y}^2=\tfrac{1}{4})=0 \qquad 0\le\bar{y}\le\frac{1}{2}\ , \quad 0\le\bar{x}\le\frac{1}{2}\ ,$$

$$\partial\bar{T}\,(\bar{x},0)/\partial\bar{y}=0\ , \qquad \frac{1}{2}<\bar{x}\le L/D\ ,$$

$$\partial\bar{T}\,(\bar{x},H/2D)/\partial\bar{y}=0\ , \qquad -N/D\le\bar{x}\le L/D\ ,$$

$$\partial\bar{T}\,(L/D,\bar{y})/\partial\bar{x}=D/L\ , \quad 0\le\bar{y}\le H/2D$$

where $\bar{x}=x/D$, $\bar{T}_\infty=\lambda_s(T_\infty-T_w)/\dot{q}''_{f\ell}\,L$ and the products Pe $\bar{U}$ and Pe $\bar{V}$ account for the increase in the characteristic (mean) velocity with $\bar{x}$ at constant mass flux. The problem was discretized by using first central differences [12] and solved employing Gauss-Seidel iteration on a PDP 11/34 mini-computer. The criterion set for convergence was $(\bar{T}_{new}-\bar{T}_{old})_{max}\le$ Tol where Tol is a prescribed tolerance, 10^{-6}, and the subscript, max, denotes that the value in the parenthesis is the maximum over all the grid points. A square grid corresponding to six nodes per diameter was used. When the grid spacing was halved, the dimensionless temperature varied by less than 2%. As a check on the numerics, the previous analytic problem of Bi = 0, U = constant, V = 0, and T = T_w at the plane of the cooling coil, was solved with < 1% difference from Eq. (8).

In this problem $\bar{T}(\bar{x},\bar{y},H/D,L/D,Pe,N/D,\bar{T}_\infty)$ with the variables listed in their approximate order of importance. Wide reasonable variations of N/D and $\bar{T}_\infty$ had negligible effect on the temperature field downstream of the coil. Figure 8 shows the surface temperature as a function of $\bar{y}$, parameterized in H/D, L/D and Pe. The temperature is normalized on the simple case surface temperature, Fig. 6, to isolate the effects of coil geometry. The primary effect lowering

the surface temperature is the nearness of the cold boundary at $\bar{x} + \bar{y} = \frac{1}{4}$ rather than $\bar{x} = 0$. As H/D decreases, more of the cell is filled with the cold boundary and $\bar{T}_u$ drops. As L/D decreases, the surface comes closer to this cold boundary and again $\bar{T}_u$ drops. If $L/D \geq \bar{x}_{min}$ in Fig. 4, the surface temperature is uniform across the cell. For small L/D, the temperature dips over the cool coil. As Pe number increases, convective effects counter conduction and the surface temperature increases. The Pe = 0.1 results were found to hold for all $Pe \leq 0.1$. Note that planes of symmetry exist at $\bar{y} = 0$, the tube center, and $\bar{y} = H/2D$. The maximum variation of the temperature across the surface occurs for large H/D and small L/D, the very conditions excluded by the velocity flatness constraints of Fig. 4. The magnitude of the surface temperature variation, $\lesssim 1\%$, may be effected by the artificially imposed constant surface flux condition.

Figure 9 shows the average of the surface temperature in Fig. 8 as a function of L/D parameterized in H/D and Pe. Again, the Pe = 0.1 result applies to all $Pe \leq 0.1$. The H/D = 4.8 case shows that as H/D increases beyond a certain value, which is a weak function of Pe, the simple case surface temperature is exceeded. This is an effect of coil geometry; the plane on which the "average" upstream temperature is T_w as moved to $\bar{x} < 0$ due to the wide separation between the tubes. It is useful that for most of the parameter range permitted by Fig. 4, the simple surface temperature, Fig. 6, is accurate to within $\pm$ 10%.

Conclusions

In summary, the detailed velocity field around the cooling coil in the sintered disk of a Kaskan type flat flame burner has been found from a potential flow analogy using the method of images. This velocity field has been used in

the energy equation to numerically find the temperature field around the coil within the disk. Simpler limiting cases of both fields are discussed. From these analyses the following conclusions are drawn:

1) The velocity field, $S/U_\infty(x/D, y/D)$, is strongly influenced by the diameter of the coil tube, D, and the distance between tube centers in the spiraled coil, H. It is independent of gas and sinter properties. Figure 4 gives the proper separation between the plane of the coil and the burner surface, L, to achieve a flat velocity profile in the exit plane of the disk. Larger separation would defeat the purpose of the burner as a heat sink while smaller separation introduces the wake of the coil into the flame. As a rough guide, $L/D \sim 1 + 0.5\ H/D$, in the practical range $1.5 \lesssim H/D \lesssim 4.5$. The smaller are D and H, the shorter is the coil wake.

2) The nondimensional temperature field, $\bar{T} = \lambda_s(T - T_w)/\dot{q}''_{f\ell}L$, is in general a function of Pe, L/D, H/D, L/r_b, Bi, T_∞ and N/D. There is a negligible dependence on the last two parameters and only a weak dependence on Bi and L/r_b provided $Bi < 1$ and $L/r_b < 0.3$ as is typical for practical burners. If H/D and L/D are related by the constraint of Fig. 4, the temperature field is reasonably approximated by the simpler result, Eq. (8). If in addition $Pe \leq 0.1$, $\bar{T}_u = 1$. More accurate surface temperatures are given by Fig. 9.

In the future, this analysis within the burner disk needs to be properly coupled to the detailed fields in the flame, i.e., the $\dot{q}''_{f\ell}$ condition should be replaced with more specific fuel and flow conditions. Also, in the downstream region, the array of gas jets emanating from the porous surface merits detailed study. Alternatives to sintering should be considered, e.g., soldering the coil to the lower disk surface may be as effective vis a´vis the thermal and flow fields.

References

1. Kaskan, W. E., "The Dependence of Flame Temperature on Mass Burning Velocity," 6th Symposium (Intl.) on Combustion, The Combustion Institute, p. 134 (1956) see also Combustion and Flame 4, pp. 285-288 (1960).

2. Toossi, R., "Physical and Chemical Properties of Combustion Generated Soot," Lawrence Berkeley Laboratory, Report LBL 7820, 145 p. (1978).

3. Burns, P. J., Chow, L. C. and Tien, C. L., "Convection in a Vertical Slot Filled with Porous Insulation," Int. J. Heat Mass Transfer 20, pp. 919-926 (1977).

4. Weinbaum, S. and Wheeler, H. L., "Heat Transfer in Sweat-Cooled Porous Metals," J. of Appl. Phys. 20, pp. 113-122 (1949).

5. Muskat, M., The Flow of Homogeneous Fluids Through Porous Media, McGraw Hill, New York, p. 55 (1937).

6. Milne-Thompson, L. M., Theoretical Hydrodynamics, MacMillan, New York, p. 154 (1960).

7. Toussaint, A., Aerodynamic Theory, (F. W. Durand, ed.) J. Springer, Berlin, Vol. III, p. 309 (1934).

8. Ferguson, C. R. and Keck, J. C., Combustion and Flame 34, pp. 85-98 (1979).

9. Carrier, G. F., Fendell, F. E. and Bush, W. B., "Stoichiometry and Flameholder Effects on a One-Dimensional Flame," Combust. Sci. and Tech. 18, pp. 33-46 (1978).

10. Kihara, D. H., Fox, J. S. and Kinoshita, C. M., "Temperature and Velocity Non-Uniformity in Edge Cooled Flat Flame Burners," Combust. Sci. and Tech. 11, pp. 239-246 (1975).

11. Botha, J. P. and Spalding, D. B., "The Laminar Flame Speed of Propane-Air with Heat Extraction from the Flame," Proc. Roy. Soc. A225, p. 71 (1954).

12. Forsythe, G. E. and Wasow, W. R., Finite Difference Methods for Partial Differential Equations, J. Wiley, New York, p. 184 (1960).

Figure Captions

Figure 1 — Schematic for flow through porous disk for velocity problem. Dashed lines separate identical cells. Symmetry allows consideration of only the cross-hatched region.

Figure 2 — Streamlines for H/D = 2.0, i.e., width of free space = coil diameter for cylinder between walls of symmetry cell.

Figure 3 — Dimensionless speed for H/D = 2.0. Solid lines depict constant speed contours. Long dashed line is the deformed coil contour. Short dashed line is the real coil contour. $(S/U_\infty)_{max} = 2.55$ at (0,0.492). Region shown is the cross-hatched area of Fig. 1. The $\bar{x}$ and $\bar{y}$-axes, as well as the line $\bar{y} = 1.0$, are lines of symmetry.

Figure 4 — Dimensionless downstream distance required for S to decay to $(1 \pm .01)\ U_\infty$ vs. dimensionless distance between coil centers. No other parameters enter the problem.

Figure 5 — Dimensionless temperature distribution in the porous disk for Bi = 0 at the rim, with slug flow and $T = T_w$ in the plane of cooling coil.

Figure 6 — Dimensionless surface temperature as a function of Peclét No. for the same conditions as Fig. 5.

Figure 7 — Dimensionless surface temperature with respect to ambient temperature as a function of aspect ratio and Biot No. for slug flow, $P_e = 0.1$ and $T_w' = -0.05$ specified in the plane of the cooling coil.

Figure 8 Dimensionless surface temperature normalized on the slug flow surface temperature of Fig. 6 vs. distance across a half-cell of the cooling coil (see Fig. 1). Symmetry exists about the origin which is on the center of a coil. A second plane of symmetry is reached when $\bar{y} = H/2D$, the mid-point between coil centers. The relative closeness of the cold boundary causes the small temperature dip directly over the coil.

Figure 9 Average dimensionless surface temperature, $\bar{T}_{u,ave} = D/H \int_o^{H/D} \bar{T}_u \, d\bar{y}$, normalized on the slug flow surface temperature vs. dimensionless distance from the surface to the plane of the coil. The surface temperature is within $\pm$ 10% of the simplest solution for $L/D > 3.5$.

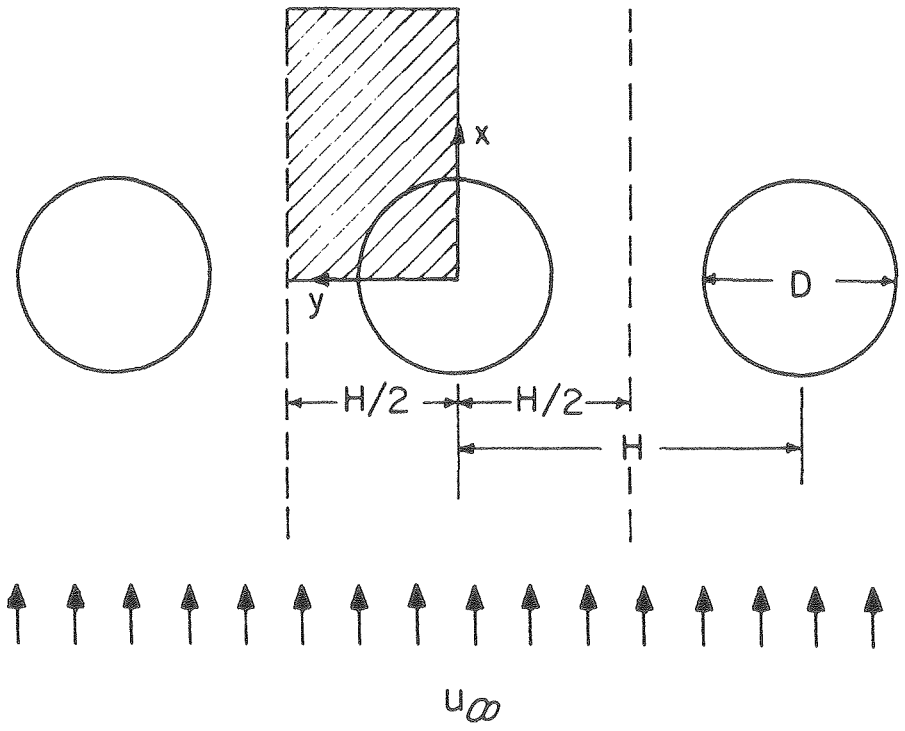

Fig. 1

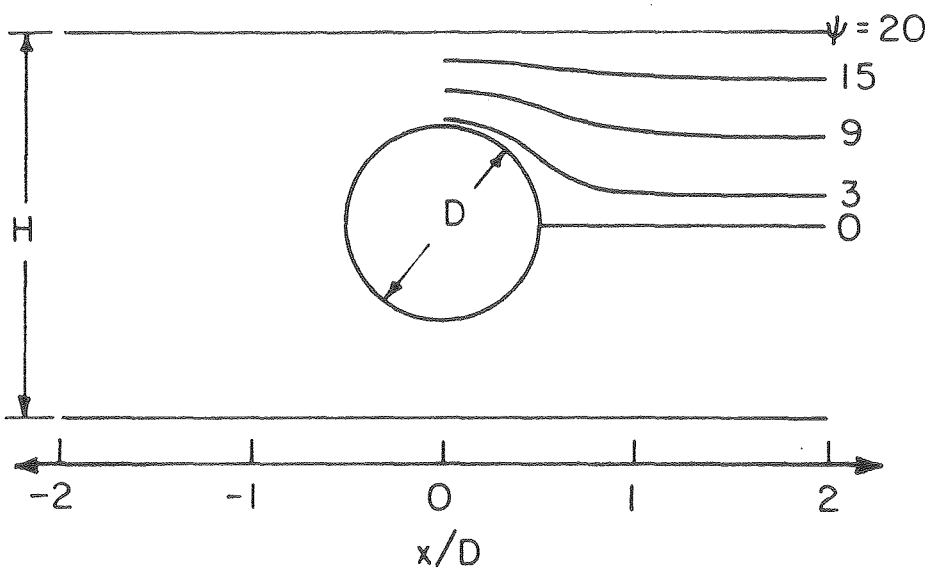

Fig. 2

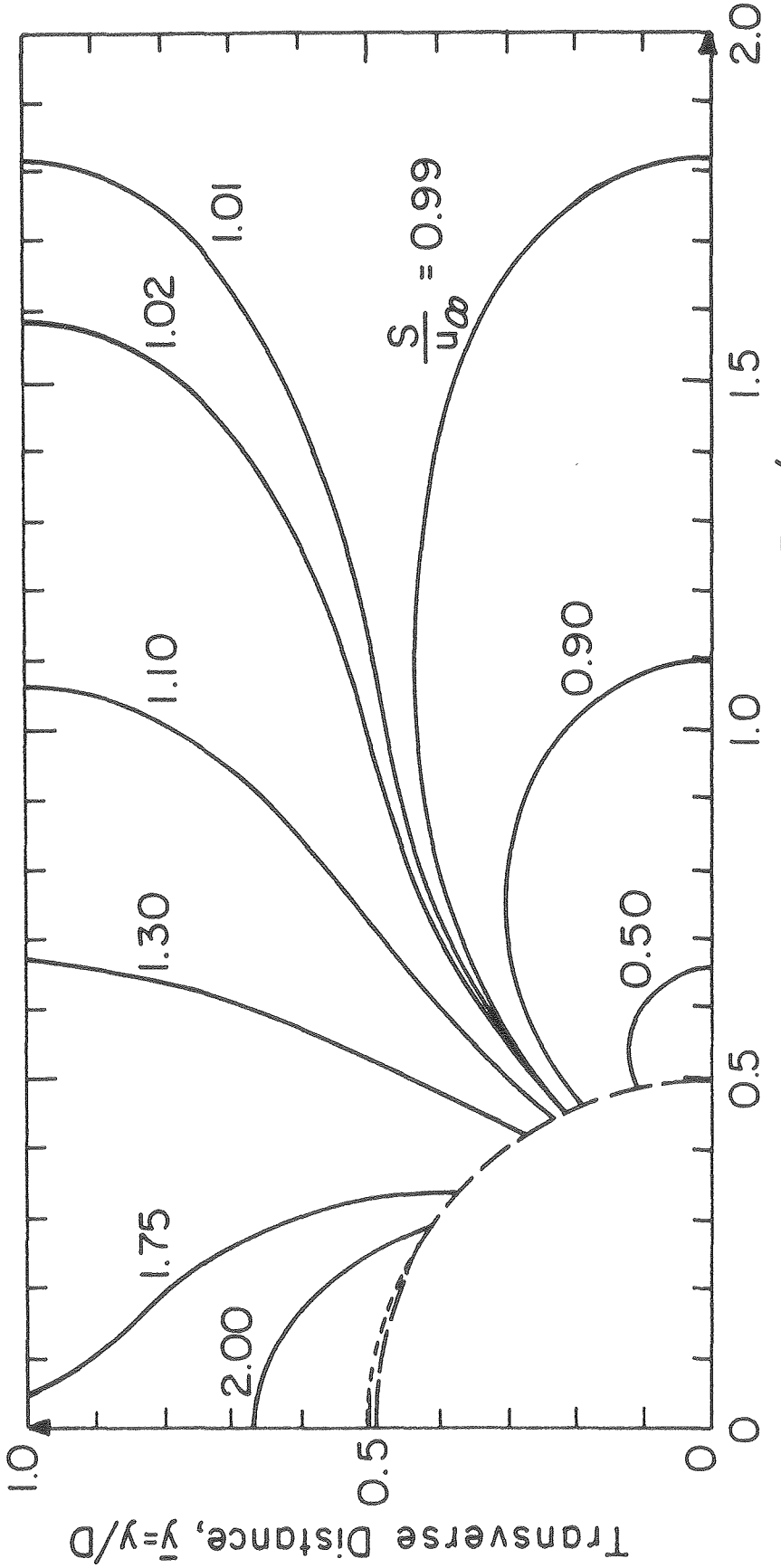
Transverse Distance, $\bar{y}=y/D$
Downstream Distance, $\bar{x}=x/D$
$\frac{S}{u_\infty}=0.99$
1.01
1.02
1.10
1.30
1.75
2.00
0.90
0.50
0
0.5
1.0
1.5
2.0

Fig. 3

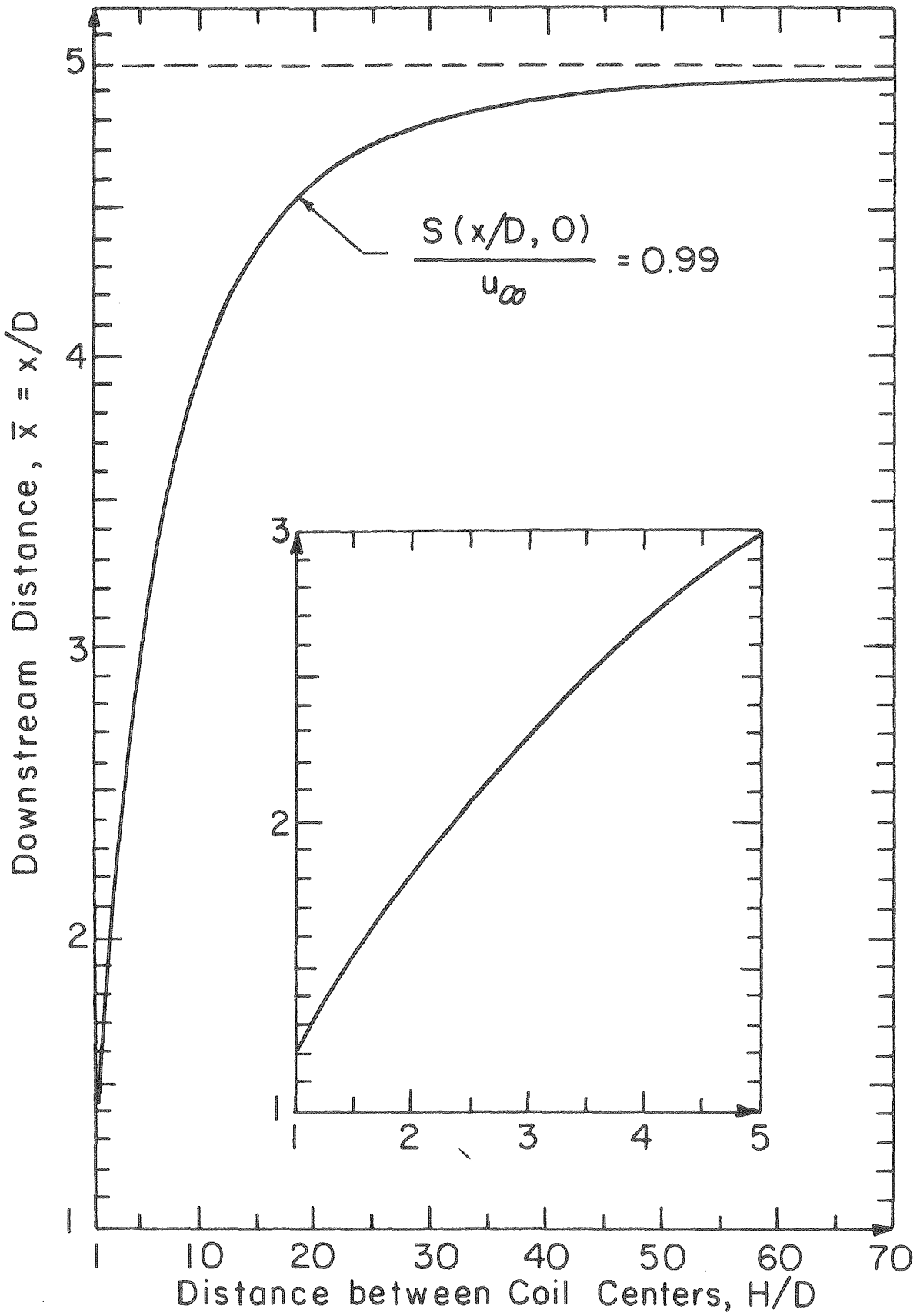
Downstream Distance, $\bar{x} = x/D$
$\frac{S(x/D, 0)}{u_\infty} = 0.99$
Distance between Coil Centers, H/D
1
2
3
4
5
10
20
30
40
50
60
70

Fig. 4

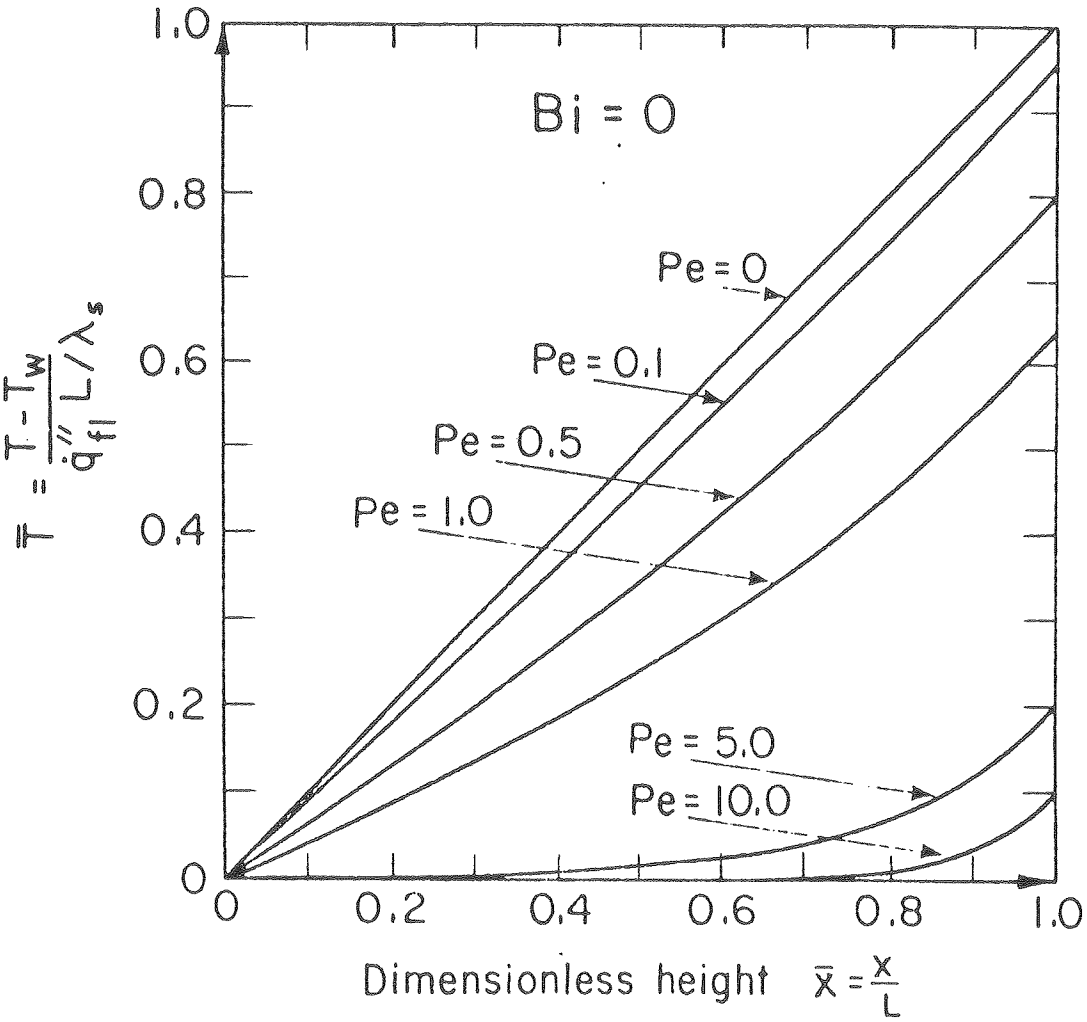
Bi = 0
Pe = 0
Pe = 0.1
Pe = 0.5
Pe = 1.0
Pe = 5.0
Pe = 10.0
$T = \frac{T - T_w}{\dot{q}''_{fl} L / \lambda_s}$
Dimensionless height $\bar{x} = \frac{x}{L}$
0
0.2
0.4
0.6
0.8
1.0

Fig. 5

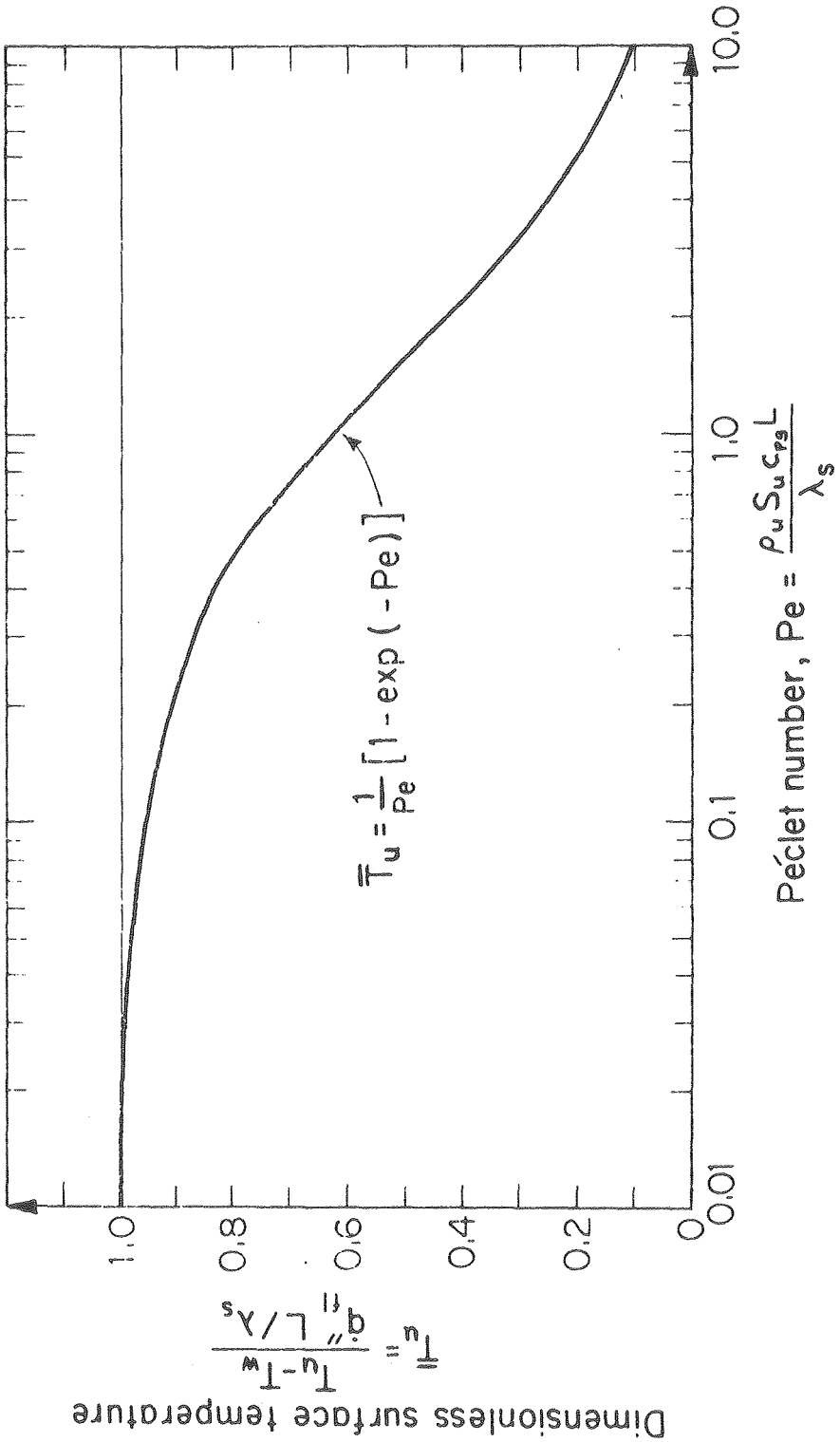
Dimensionless surface temperature
$\bar{T}_u = \frac{T_u - T_w}{q''_{ii} L/\lambda_s}$
1.0
0.8
0.6
0.4
0.2
0
0.01
0.1
1.0
10.0
Péclet number, Pe = $\frac{\rho_u S_u c_{pg} L}{\lambda_s}$
$\bar{T}_u = \frac{1}{Pe}[1 - \exp(-Pe)]$

Fig. 6

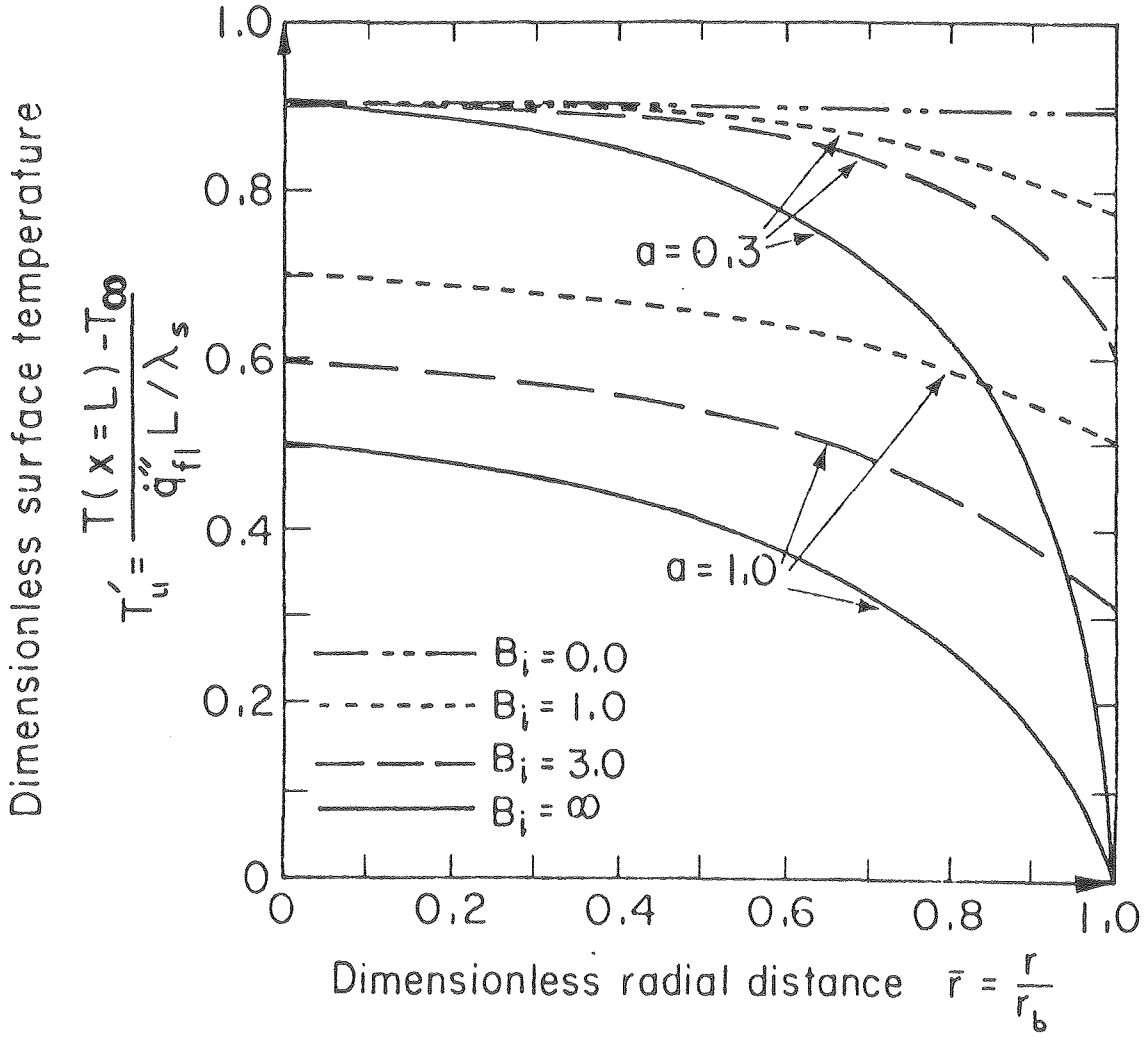
Dimensionless surface temperature
$T'_u = \frac{T(x=L)-T_\infty}{\dot{q}''_{fl} L/\lambda_s}$
1.0
0.8
0.6
0.4
0.2
0
0
0.2
0.4
0.6
0.8
1.0
a = 0.3
a = 1.0
$B_i = 0.0$
$B_i = 1.0$
$B_i = 3.0$
$B_i = \infty$
Dimensionless radial distance $\bar{r} = \frac{r}{r_b}$

Fig. 7

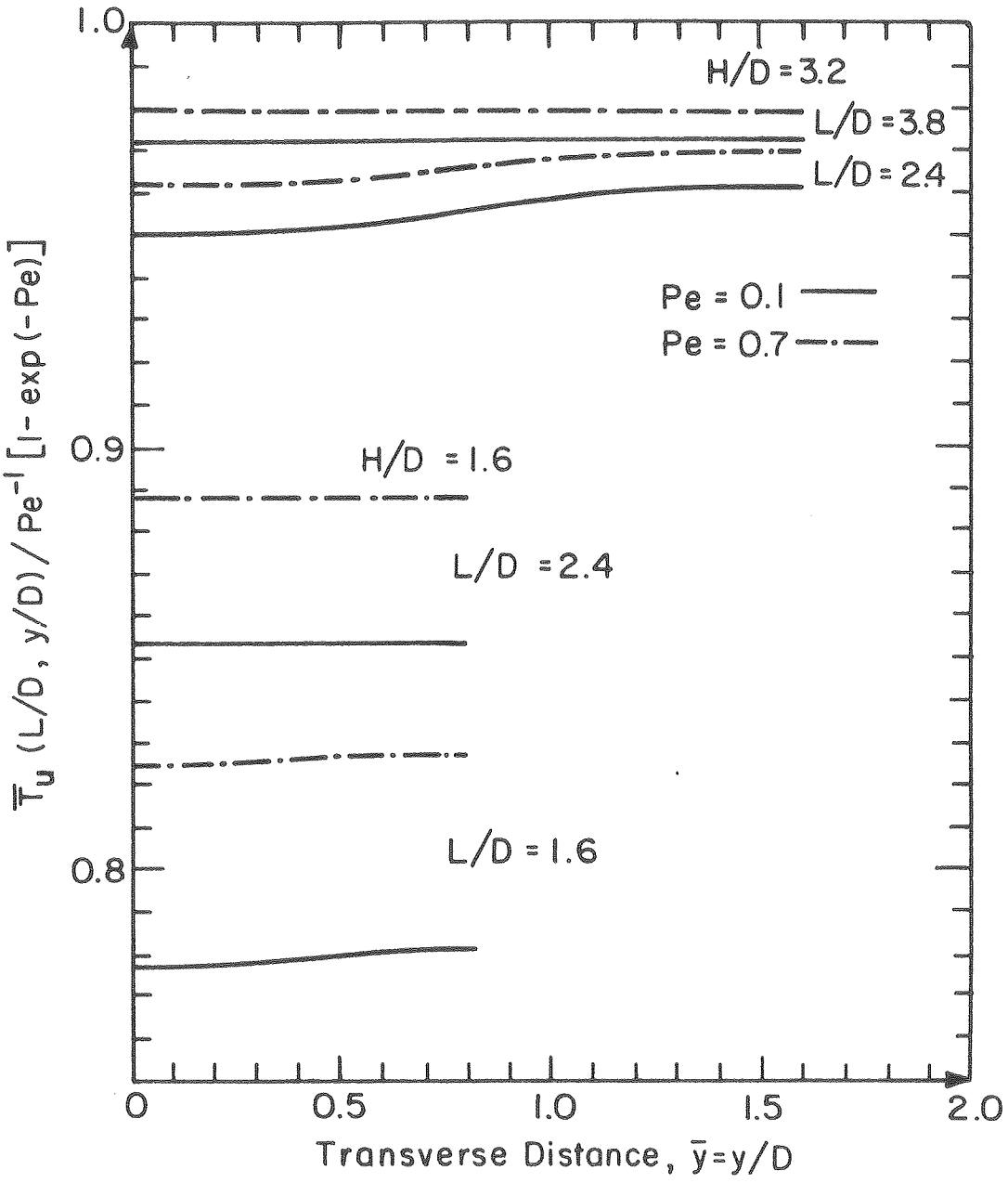
1.0
0.9
0.8
H/D = 3.2
L/D = 3.8
L/D = 2.4
Pe = 0.1
Pe = 0.7
H/D = 1.6
L/D = 2.4
L/D = 1.6
$\overline{T}_u$ (L/D, y/D) / Pe^{-1} [1 - exp (-Pe)]
0
0.5
1.0
1.5
2.0
Transverse Distance, $\bar{y}$ = y/D

Fig. 8

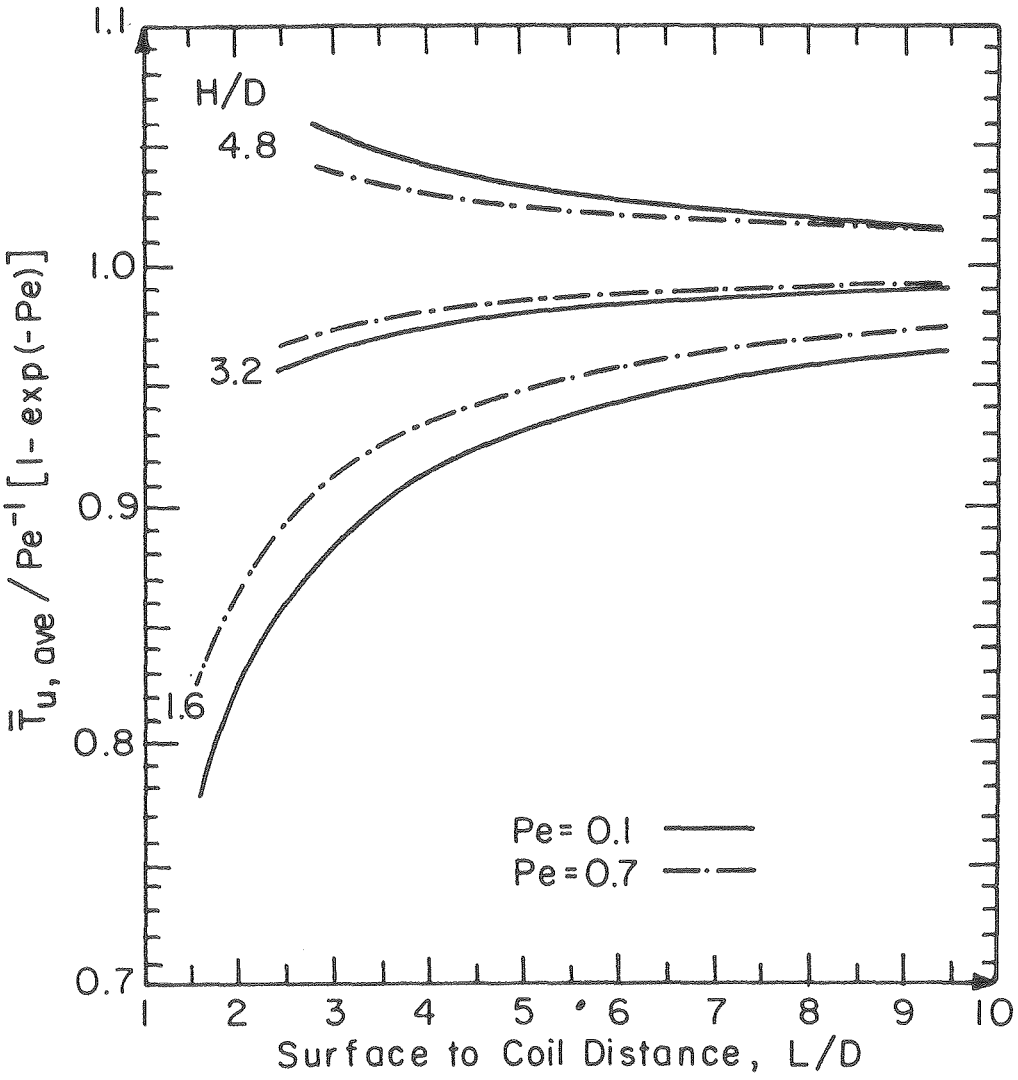
1.1
1.0
0.9
0.8
0.7
H/D
4.8
3.2
1.6
Pe= 0.1
Pe= 0.7
1 2 3 4 5 6 7 8 9 10
Surface to Coil Distance, L/D
$\bar{T}_{u,ave} / Pe^{-1}[1-exp(-Pe)]$

Fig. 9

Nomenclature

a aspect ratio, L/r_b

Bi Biot number, hr_b/λ_s

c_p specific heat capacity

D outside diameter of cooling coil tube

h heat transfer coefficient at burner periphery

H distance between coil centers

L downstream distance from plane of coil to porous disk surface

N upstream distance from plane of coil to porous disk entrance

Pe Peclét number, $\rho_u S_u c_{pg} L/\lambda_s$

Pr modified Prandtl number, $(\mu c_p)_g/\lambda$

$\dot{q}''_{fl}$ heat flux from flame

S speed

T temperature

T' dimensionless temperature, $\lambda_s(T-T_\infty)/\dot{q}''_{fl}L$

$\overline{T}$ dimensionless temperature, $\lambda_s(T-T_w)/\dot{q}''_{fl}L$

U velocity in x-direction

$\overline{U}$ dimensionless velocity in x-direction, U/U_∞ or U/S_u

V velocity in y-direction

$\overline{V}$ dimensionless velocity in y-direction, V/U_∞ or V/S_u

x downstream distance from center plane of coil

$\overline{x}$ dimensionless downstream distance, x/D or x/L

y transverse distance from center plane of coil

$\overline{y}$ dimensionless transverse distance, y/D

Greek

ε permeability of porous disk

λ_s thermal conductivity of solid (porous medium)

μ viscosity

ρ density

ψ stream function

Subscripts

w water

b burner

∞ ambient, upstream bondary

u unburned gas at surface of disk

g gas

s solid (porous medium)